

# Influence of strain on the atomic and electronic structure of manganite films

Q. Qian<sup>a,\*</sup>, T.A. Tyson<sup>a,\*</sup>, M. Deleon<sup>a</sup>, C.-C. Kao<sup>b</sup>, J. Bai<sup>c</sup>, A.I. Frenkel<sup>d</sup>

<sup>a</sup>Department of Physics, New Jersey Institute of Technology, Newark, NJ 07102, USA

<sup>b</sup>Brookhaven National Laboratory, Upton, Long Island, NY 11973, USA

<sup>c</sup>Oak Ridge National Laboratory, Oak Ridge, TN 37831, USA

<sup>d</sup>Physics Department, Yeshiva University, New York, NY 10016, USA

Received 2 April 2006; received in revised form 5 December 2006; accepted 16 December 2006

## Abstract

A study of the long-range, local and electronic structure of  $\text{Nd}_{0.5}\text{Sr}_{0.5}\text{MnO}_3$  films of varying thickness between 500 and 2000 Å has been performed. Local structure measurements at the Sr K-edge reveal a reduction of the Mn–O–Mn bond angles in films below 1000 Å. Spin-polarized measurements reveal splitting of the Mn 3d  $e_g$  state in the strained region of the films and are consistent with a two-layer model for thick films with a relaxed undistorted layer on top of a strained structurally distorted layer near the substrate.

© 2007 Elsevier Ltd. All rights reserved.

PACS: 68.55.–a; 61.10.Ht; 72.15.Gd; 61.10.–i; 81.15.Fg

Keywords: C. XRD

## 1. Introduction

Due to the interest in understanding the intriguing magnetic property and transport properties, colossal magnetoresistance (CMR) perovskite manganites have attracted a great deal of attention [1]. Although there is evidence that the properties and the complex phase diagrams of CMR manganites are driven by the combined charge, spin, and orbital degrees of freedom in the system, the details of the coupling and the consequences of them are still an active area of research. Strain in films has also opened the door to understand the CMR property based on growing thin CMR films on substrates with different lattice spacing [2,3] and varying thickness.

Thin manganite films display properties different from those of bulk materials. Jin et al. [2] conducted a systematic experimental study of the effect of the thickness dependence on the magnetotransport properties of thin films,

which attracted following research by others [3,4]. The common feature found in this research is that the metal–insulator (MI) transition is suppressed in very thin films. Detailed magnetic studies have also been performed [5–9]. O'Donnell et al. [9] suggested that the magnetic anisotropy in films seen in many experiments is dominated by strain-induced anisotropy leading to easy axis which occurs parallel to or normal to the film plane depending on substrate-induced compression or tension. Millis et al. [10] made the first attempt at quantifying the role of strain in these materials and showed that Curie temperature  $T_c$  is extremely sensitive to biaxial strain and that  $T_c$  reduction is quadratic in the Jahn Teller (JT) distortion [11]. Calculation of the phase diagram of tetragonal manganites [12] also showed that magnetic degrees of freedom can be indirectly controlled by lattice distortions via orbital degrees of freedom. Specifically, the author argued that by changing the  $c/a$  ratio the Mn 3d  $e_g$  orbital (3d orbital is split to  $t_{2g}$  and  $e_g$  in crystal symmetry) extending along the elongated Mn–O bond is preferentially occupied.

In early work on  $\text{Nd}_{0.5}\text{Sr}_{0.5}\text{MnO}_3$  films, Prellier et al. [13] found that a metallic state is induced in thick films while

\*Corresponding authors.

E-mail addresses: [qqian@njit.edu](mailto:qqian@njit.edu) (Q. Qian), [tyson@adm.njit.edu](mailto:tyson@adm.njit.edu) (T.A. Tyson).

thin films remain insulating- with no insulator–metal transition at  $\sim 150$  K as in bulk [14]. Our previous work on  $\text{Nd}_{0.5}\text{Sr}_{0.5}\text{MnO}_3$  films showed that in this system there is an optimal strain value that will produce materials with high metallic properties. In thin films, the strain induces JT distortions that stabilize the charge-ordered phase [15]. In order to understand the atomic and electronic structure, in this paper we present the combined measurement of the X-ray diffraction (XRD), extended X-ray absorption fine structure (EXAFS) and spin-polarized X-ray absorption near-edge spectrum (SPXANES) in  $\text{Nd}_{0.5}\text{Sr}_{0.5}\text{MnO}_3$  films of varying thickness. EXAFS measurements reveal severe buckling of the Mn–O–Mn bond in films below  $1000 \text{ \AA}$ . We find (from SPXANES) that the thick films exhibit undistorted top layers covering structurally distorted layers near the substrate.

## 2. Experimental methods

Films of  $\text{Nd}_{0.5}\text{Sr}_{0.5}\text{MnO}_3$  were grown *in situ* using the pulsed laser deposition technique [16]. Substrates used were  $\text{LaAlO}_3$  (100) (pseudocubic with  $a = 3.791 \text{ \AA}$ ). The sample preparation is described in Ref. [13]. We note that  $\text{Nd}_{0.5}\text{Sr}_{0.5}\text{MnO}_3$  has a  $\text{Pnma}$  space group with lattice parameters  $a = 5.434 \text{ \AA}$ ,  $b = 7.634 \text{ \AA}$ , and  $c = 5.477 \text{ \AA}$  [14]. This corresponds to a pseudocubic cell with  $a = 3.845 \text{ \AA}$ . Hence the film will be compressively strained by the substrate ( $\sim 1.4\%$  lattice mismatch). Laboratory XRD studies showed that the films were (101) oriented. Rutherford Backscattering measurements confirm that the films have the same composition as bulk materials. Mn  $K_\beta$  emission measurements [17] were also performed on the films and reveal that no change in the valence occurred as a function of film thickness (Fig. 1). The synchrotron XRD experiments described below were performed on the Oak Ridge National Laboratory's beamline X14A at the National Synchrotron Light Source (NSLS) at the Brookhaven National Laboratory (BNL). The X-ray energy was set to  $8.0468 \text{ keV}$  ( $\lambda = 1.5406 \text{ \AA}$ ). Spin-polarized Mn

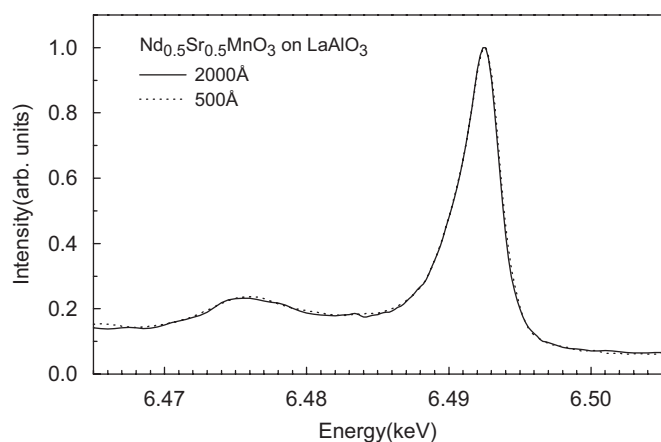


Fig. 1. X-ray  $K_\beta$  emission spectra of  $\text{Nd}_{0.5}\text{Sr}_{0.5}\text{MnO}_3$  films. The solid line is from the  $2000 \text{ \AA}$  film and the dashed line is from the  $500 \text{ \AA}$  film. Note that there is no valence shift between these films.

K-edge absorption spectra in fluorescence mode were measured on NSLS beamline X21A at BNL. Measurements were made for films in two orientations: one with the beam  $E$ -vector nearly perpendicular ( $E$ -vector  $\sim 10^\circ$  from the surface normal) to the surface and one with the  $E$ -vector  $45^\circ$  with the surface plane of the film. The near-edge spectra were area normalized. Periodically, the beamline monochromator (two independent  $\text{Si}(220)$  pairs comprising a four-bounce system) was calibrated using an Mn foil. No energy shift larger than  $0.10 \text{ eV}$  was found. The Sr K-edge EXAFS spectra were measured at NSLS beamline X16C. The film samples were spun while held at  $45^\circ$  in order to suppress diffraction peaks from the sample and substrate. EXAFS data reduction followed standard procedures [18]. The powder sample was measured at the Advanced Photon Light Source MR-CAT undulator beamline. All measurements were carried out at room temperature.

## 3. Results and discussion

In Fig. 2, we show the diffraction profiles for (242) plane reflections on  $\text{Nd}_{0.5}\text{Sr}_{0.5}\text{MnO}_3$  film which intersects the surface (101) oriented at  $\sim 45^\circ$ . For the  $500 \text{ \AA}$  films (dashed line), the line can be fitted by two Gaussian peaks, which suggests a two-layer film where one component dominates in volume. This result is consistent with the

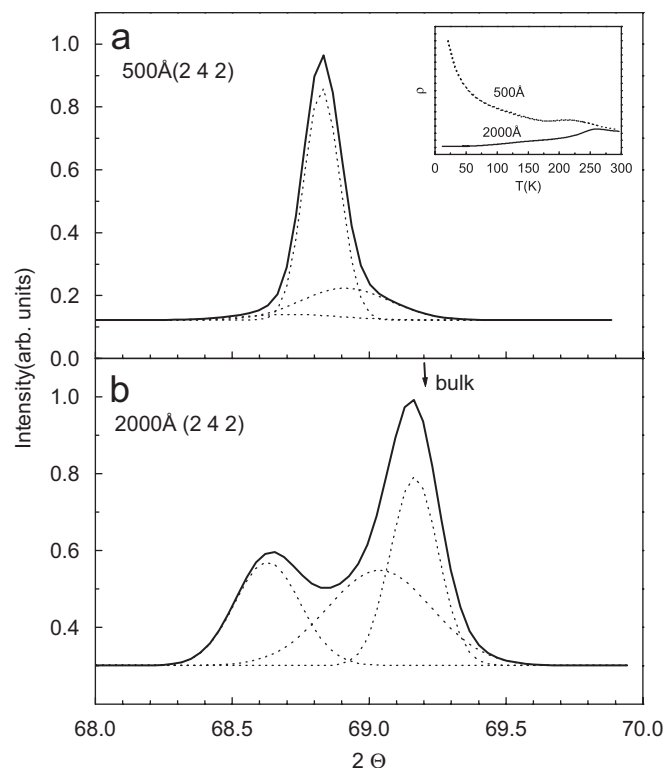


Fig. 2. X-ray-diffraction  $\theta$ – $2\theta$  scans of  $\text{Nd}_{0.5}\text{Sr}_{0.5}\text{MnO}_3$  films for the (242) plane ( $\sim 45^\circ$  to the surface plane (101)). The solid line is the experimental measurement and dashed lines are Gaussian peak fits. Panels (a) and (b) are for the  $500$  and  $2000 \text{ \AA}$  films, respectively. The inset displays the resistivity data.

detailed in-plane and out-of-plane XRD study conducted previously [15]. By comparison, the 2000 Å film shows two significant peaks and an additional peak in between the main peaks indicating a progressive transition for the strained region near the substrate to a more relaxed top region with lattice parameter near the bulk value. It is clear that the dominant peak for the 500 Å film is at low-angle side (higher  $d$ -spacing), while it is at high-angle side (lower  $d$ -spacing) in the 2000 Å film. This supports a model in which the main layer is near the substrate for the 500 Å film, but the main layer is at the surface for the 2000 Å film. The point to note is that the thick film is composed of two dominant components with the main peak close to the bulk  $d_{hkl}$  value. The thin film has two components also but with one dominating. The measurements are at 45°, hence we are seeing a mixture on in-plane and out-of-plane strained atomic planes. The components of both films have different  $d$ -spacings. This leads to the main peak position being different in the two films. The two-layer mode is consistent with the in-plane and out-of-plane XRD measurements conducted on these films which we reported previously [15]. The extracted lattice parameters are given in Table 1, for the peaks of Fig. 2 combined with the in-plane and out-of-plane results (in [15]).

In order to correlate the changes in the long-range structure (found in the XRD measurements) with changes in the local structure about the average Mn site, we measured spin-polarized Mn K-edge absorption spectra of both films, for directions 45° and 10° (with electric field  $\sim$ out-of-plane). This enables us to explore distortion-induced asymmetry in the local structure. A highly structurally ordered film should exhibit weaker angular dependence than one with lower symmetry (octahedral symmetry vs. tetragonal symmetry for example).

In Fig. 3 we note that there is only a small difference between the main edges (with peak at 6.555 KeV) for both orientation and film thickness. This is consistent with our previous results [15] since here the measurements are not

orthogonal. But the difference between spin-up and spin-down channels (due to exchange interaction of photoelectron with the spin-up and spin-down densities of states) is clear for both films [19].

Here we give a qualitative discussion based on a model which we developed to determine local magnetic structure in simple perovskite manganites (see Ref [19] for complete details). A partial diagram of the transitions relevant to the pre-edge features  $a1\downarrow$  and  $a2\downarrow$  to be discussed below is given in Fig. 4. The  $a1\downarrow$  peak corresponds to transitions of an Mn 1s spin-down electron to a majority  $e_g^1$  state on a neighboring Mn site with anti-parallel moment relative to the absorbing site. The  $a2\downarrow$  peak corresponds to transitions to the next highest state of the same type, the  $e_g^2$  state. Note that by  $e_g$  we mean Mn 4p hybridized with Mn  $e_g$  and O 2p (See Ref. [19]).

At the signal-to-noise level here, it is hard to deduce any difference in the spin-up channels (from the weak satellite in the  $K_\beta$  spectrum) for different orientations with both thickness films. Fig. 5 shows the expansion of Fig. 3 at the pre-edge region labeled as “a” for the spin-down channel. For this channel (from the large peak in the  $K_\beta$  spectrum), the films 500 and 2000 Å are quite different in the region 6.540–6.543 KeV. According to our transition model developed previously (Ref. [19] and Fig. 4), the intensity  $a1\downarrow$  (at 6.541 KeV) is from a state composed of the neighboring Mn anti-parallel  $e_g^1$  state and the intensity  $a2\downarrow$  (at 6.5425 KeV) is from the neighbor Mn anti-parallel  $e_g^2$  state.

The trends seen in the spectra can be understood by a simple two-phase model for the thick film (and a single phase model for the thin film). In Fig. 6 we show a schematic of the structure (top) and the partial  $e_g$  density of states derived from the spin-down SPXANES. For the thick film the  $a1\downarrow$  feature has two components one from the top-ordered layer and the other from the near substrate distorted layer. The states are both of  $e_g$  symmetry. Due to the lowering of symmetry, the  $e_g$  state for the distorted

Table 1  
Nd<sub>0.5</sub>Sr<sub>0.5</sub>MnO<sub>3</sub> XRD results

Index	2000 Å			500 Å			Bulk (297 K) <sup>a</sup> $d$ (Å)
	$2\theta$ (deg.)	$d$ (Å)	$\varepsilon_{hkl}$ (%)	$2\theta$ (deg.)	$d$ (Å)	$\varepsilon_{hkl}$ (%)	
202 (out-plane)	46.403	1.955(7)	1.348	46.244	1.962(5) <sup>b</sup>	1.711	1.929
	47.113	1.927(7) <sup>b</sup>	−0.104	46.470	1.953(3)	1.244	
31–2 (in-plane)	62.866	1.477(11)	−0.337	63.637	1.461(2)	−1.417	1.482
	63.132	1.472(6) <sup>b</sup>	−0.675	63.735	1.459(1) <sup>b</sup>	−1.552	
1–50 (in-plane)	62.908	1.476(12)	0.408	63.681	1.460(2)	−0.680	1.470
	63.131	1.472(5) <sup>b</sup>	0.136	63.739	1.459(1) <sup>b</sup>	−0.748	
242 (45°)	68.627	1.366(3)	0.663	68.829	1.363(2) <sup>b</sup>	0.442	1.357
	69.162	1.357(3) <sup>b</sup>	0.000	68.915	1.361(6)	0.295	

Index constants  $[h, k, l]$ ,  $2\theta$  diffraction angles and  $d$  spacing determined from synchrotron XRD.  $\varepsilon_{hkl}$  is effective strain defined as  $\varepsilon_{hkl} = [d_{hkl}(\text{film}) - d_{hkl}(\text{bulk})]/d_{hkl}(\text{bulk})$ .

<sup>a</sup>Bulk parameters from Ref. [14].

<sup>b</sup>Dominant peak.

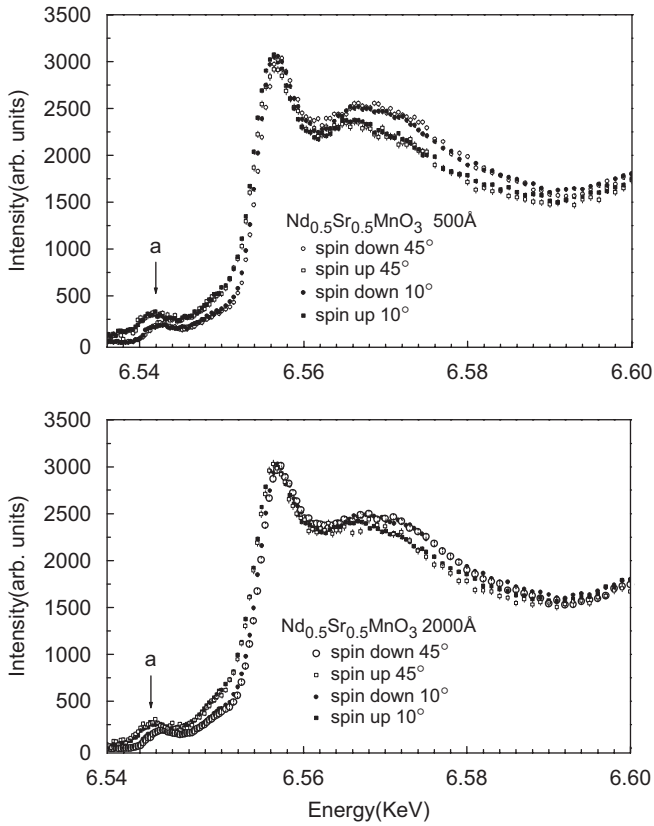


Fig. 3. SPXANES spectra of the  $\text{Nd}_{0.5}\text{Sr}_{0.5}\text{MnO}_3$  films. They are measured at an angle of the beam relative to plane of the surface ( $10^\circ$  and  $45^\circ$ ): Open (closed) circles correspond to spin-down channel measured at  $45^\circ$  (at  $10^\circ$ ); Open (closed) squares correspond to spin-up channel measured at  $45^\circ$  (at  $10^\circ$ ).

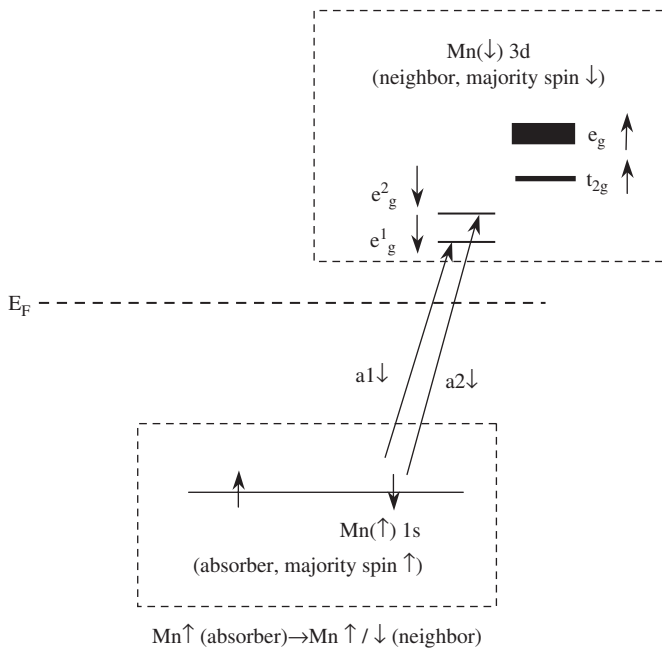


Fig. 4. A partial transition diagram of the excitations relevant to the pre-edge features labeled  $a1\downarrow$  and  $a2\downarrow$ .

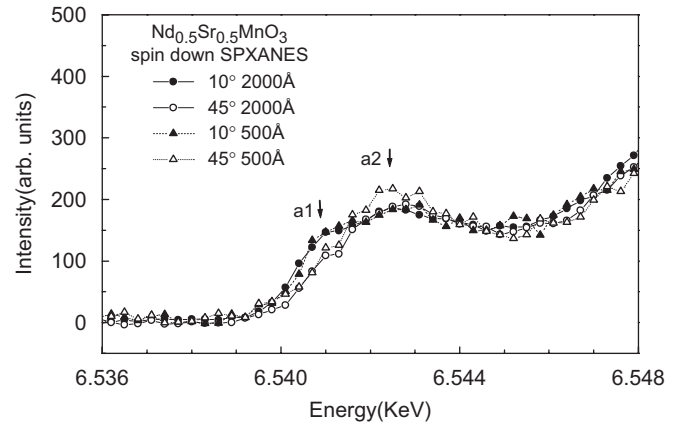


Fig. 5. Angle-dependent pre-edge SPXANES for spin-down spectra of the 500 and 2000 Å films. Open (closed) circles correspond to the spin-down channel measured at  $45^\circ$  (at  $10^\circ$ ) for the 2000 Å film. Open (closed) triangle corresponds to spin-down channel measured at  $45^\circ$  (at  $10^\circ$ ) for the 500 Å film.

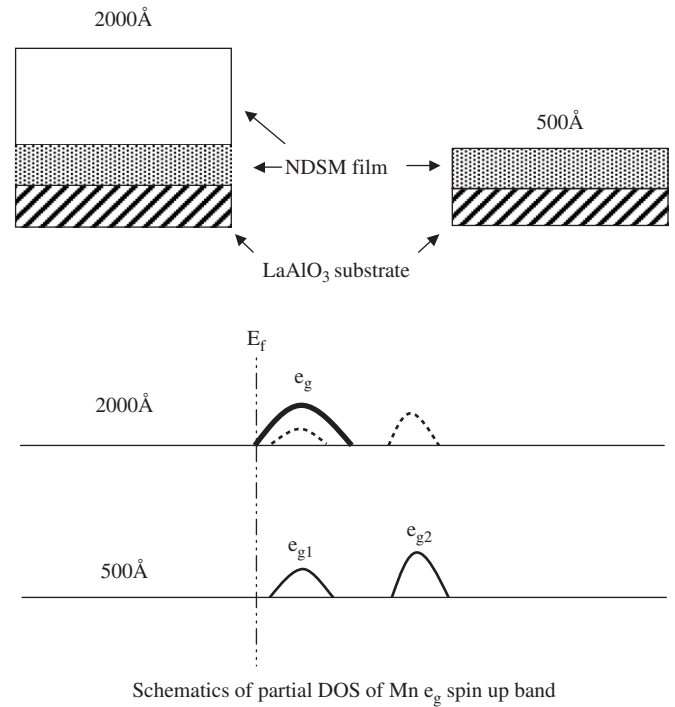


Fig. 6.  $\text{Nd}_{0.5}\text{Sr}_{0.5}\text{MnO}_3$  film structure model and schematics of Mn majority  $e_g$  band partial density of state above  $E_F$ . Top half shows the structure model of the end-member films grown on  $\text{LaAlO}_3$ . The bottom shows the Mn majority  $e_g$  band partial DOS above  $E_F$ . In the 2000 Å film, the dashed line represents the strained layer region, while the solid line represents the sole strained layer. For the 500 Å film, the solid represents the sole strained layer.

layer is split into two components called  $e_g^1$  and  $e_g^2$ . A single state remains, however, for the top undistorted layer. For the thin film only the distorted layer is present. If we assign the  $e_g^1$  state to have  $d_{3z^2-r^2}$  symmetry and the  $e_g^2$  state to have  $d_{x^2-y^2}$  symmetry, then the orientation-dependent trends can be understood. When the beam is at  $10^\circ$ , then the electric field points mainly along the sample normal.

From our previous work we found that this direction corresponded to  $z$  direction. Hence transitions to states of  $d_{3z^2-r^2}$  symmetry are probed. Rotation to  $45^\circ$  probes a mixture of states  $e_g^1$  and  $e_g^2$ . The  $a1\downarrow$  feature is pronounced in both films since at this energy, the  $e_g$  and split  $e_g^1$  states have finite density with  $z$ -polarized symmetry. For the higher  $a2\downarrow$  feature, on the split-off  $e_g^2$  state is available. Hence, only in the structurally distorted thin film there is enhanced intensity for rotation to  $45^\circ$ .

Fig. 7(a) is a simple cubic cell for  $\text{Nd}_{0.5}\text{Sr}_{0.5}\text{MnO}_3$  with the Mn atom at the center, and surrounded by six O atoms on six faces and Nd or Sr atoms are located on the corners. In Fig. 7(b) we show the Fourier Transform (FT) of the Sr K-edge EXAFS spectra for a powder sample compare with the 500, 1000 and 2000 Å films. (Note that the FT peaks are shifted to lower distance than the crystallographic position due to the central and scattering atom phase shifts.) From

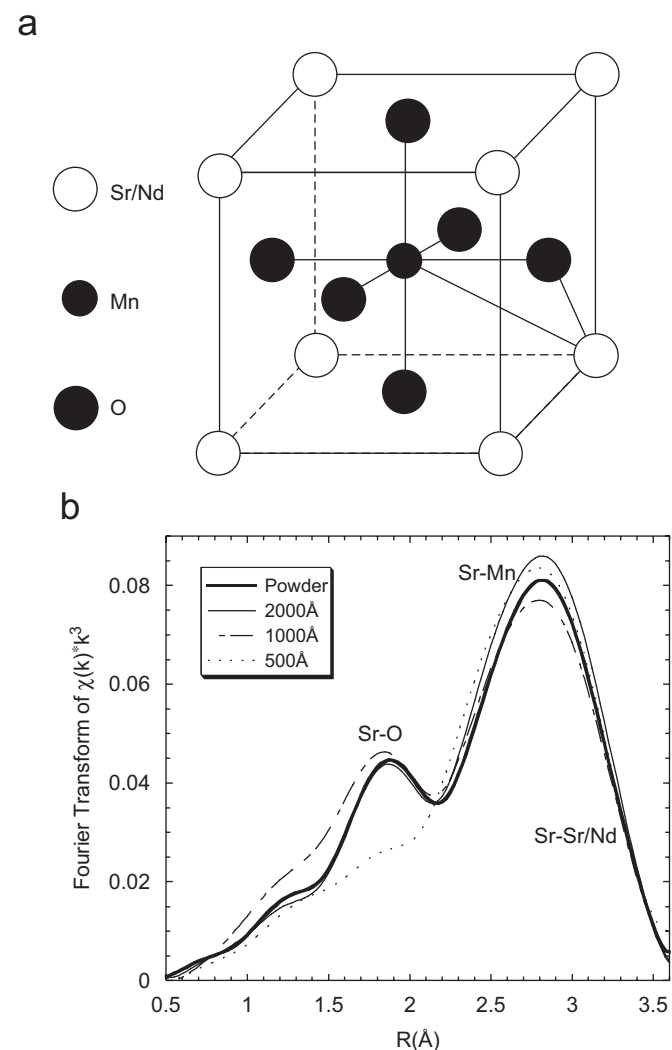


Fig. 7. (a) Illustration of structure about the Sr site based on a simple cubic perovskite structure. (b) Fourier transform of EXAFS spectra of  $\text{Nd}_{0.5}\text{Sr}_{0.5}\text{MnO}_3$  of Sr K-edge with Sr–O and Sr–Mn shells. The bold solid line is for the powder, the thin solid line is for the 2000 Å film, the dot-dash line is for the 1000 Å film and the dotted line is for the 500 Å film. Note the suppression of the Sr–O peak in the 500 Å film.

the crystal structure of the bulk materials [20], we know that the first shell about Sr is comprised of 12 O atoms with distance varying from 2.46 to 3.01 Å while the second shell is composed of 6 Mn atoms with distance varying from 3.32 to 3.34 Å. This is followed by a third shell composed of Nd and Sr atoms with distances varying from 3.81 to 3.87 Å. Note that the powder, 2000 and 1000 Å film all have a significant peak in the oxygen first shell. The absence of this peak in the 500 Å film indicates that there is a significant broadening of the Sr–O atomic distribution due to buckling of the Mn–O–Mn bond angles as would be expected for a charge-ordered state in manganites. This buckling is consistent with the asymmetry in the polarized Mn K-edge spectra reported by us previously [21]. Hence, the substrate-induced strain lock-in a buckled Mn–O–Mn configuration with weak Mn–Mn hopping leading to an insulating state.

The substrate-induced strain in the thin film produces a dominant and distorted layer in the thin film. The SPXANES reveals that the distortion splits the  $e_g$  level. The high resistivity seen in the thin film is the result of localization of the  $e_g$  electrons due to the distortion. High-resolution temperature-dependent measurements of the in-plane and out-of-plane lattice spacings across the bulk transition temperature to search for bulk-like components will be carried out. In addition, further work is needed to specify the electronic structure of the thin films. The direct comparison of our results (on these films) with resonant X-ray scattering measurements [22] of orbital ordering will be instructive.

#### 4. Summary

A study of the long-range, local and electronic structure of  $\text{Nd}_{0.5}\text{Sr}_{0.5}\text{MnO}_3$  films of varying thickness between 500 and 2000 Å has been performed. Direct evidence for a strain-induced local distortion of the  $\text{MnO}_6$  octahedra is found. Local structure measurements at the Sr K-edge reveal a reduction of the Mn–O–Mn bond angles in films below 1000 Å. Spin-polarized measurements show a strain-induced splitting of the Mn 3d  $e_g$  orbitals resulting in localization and high resistivity in the thin films. XRD measurements reveal both strained and unstrained components in the thick film while only a strained layer is found in the thin film. The combined measurements are consistent with a two-layer model for thick films with a relaxed undistorted layer on top of a strained structurally distorted layer near the substrate.

#### Acknowledgments

Data acquisition was performed at Brookhaven National Laboratory's National Synchrotron Light Source which is funded by the US Department of Energy. This work was supported by NSF grants DMR-0209243, DMR-0512196, and DMR-IMR 0216858. We acknowledge C. Cui for powder sample preparation at NJIT. We also acknowledge

W. Prellier, A. Biswas and R.L. Greene for film sample preparation at the University of Maryland which was partially supported by an NSF-MRSEC award. AIF acknowledges support by U.S. DOE Grant No. DE-FG02-05ER36184.

## References

- [1] Y. Tokura, Y. Tomioka, *J. Magn. Magn. Mater.* 200 (1999) 1 and references therein;  
J.M. Coey, M. Verit, S. von Molnar, *Adv. Phys.* 48 (1999) 167 and references therein.
- [2] S. Jin, T.H. Tiefel, M. McCormack, H.M. O'Bryan, L.H. Chen, R. Ramesh, D. Schurig, *Appl. Phys. Lett.* 67 (1995) 557.
- [3] M.G. Blamire, B.-S. Teo, J.H. Durrell, N.D. Mathur, Z.H. Barber, J.L. McManus Driscoll, L.F. Cohen, J.E. Evetts, *J. Magn. Magn. Mater.* 191 (1999) 359.
- [4] J.Z. Sun, D.W. Abraham, R.A. Rao, C.B. Eom, *Appl. Phys. Lett.* 74 (1999) 3017.
- [5] Y. Suzuki, H.Y. Hwang, S.-W. Cheong, R.B. van Dover, *Appl. Phys. Lett.* 71 (1997) 140.
- [6] X.W. Wu, M.S. Rzchowski, H.S. Wang, Qi. Li, *Phys. Rev. B* 61 (2000) 501.
- [7] H.S. Wang, Qi. Li, Kai. Liu, C.L. Chien, *Appl. Phys. Lett.* 74 (1999) 2212;  
H.S. Wang, Qi. Li, *Appl. Phys. Lett.* 73 (1998) 2360.
- [8] T.K. Nath, R.A. Rao, D. Lavric, C.B. Eom, L. Wu, F. Tsui, *Appl. Phys. Lett.* 74 (1999) 1615.
- [9] J. O'Donnell, M.S. Rzchowski, J.N. Eckstein, I. Bozovic, *Appl. Phys. Lett.* 72 (1998) 1775.
- [10] A.J. Millis, T. Darling, A. Migliori, *J. Appl. Phys.* 83 (1998) 1588.
- [11] A.J. Millis, et al., unpublished.
- [12] Z. Fang, I.V. Solovyev, K. Terakura, *Phys. Rev. Lett.* 84 (2000) 3169.
- [13] W. Prellier, A. Biswas, M. Rajeswari, T. Venkatesan, R.L. Greene, *Appl. Phys. Lett.* 75 (1999) 397.
- [14] H. Kawano, R. Kajimoto, H. Yoshizawa, Y. Tomioka, H. Kuwahara, Y. Tokura, *Phys. Rev. Lett.* 78 (1997) 4253;  
H. Kuwahara, Y. Tomioka, A. Asamitsu, Y. Moritomo, Y. Tokura, *Science* 270 (1995) 961;  
H. Kawano, Ph.D. Thesis.
- [15] Q. Qian, T.A. Tyson, C.-C. Kao, W. Prellier, J. Bai, A. Biswas, R.L. Greene, *Phys. Rev. B* V63 (2001) 224424.
- [16] H.L. Ju, C. Kwon, Q. Li, R.L. Greene, T. Venkatesan, *Appl. Phys. Lett.* 65 (1994) 2108.
- [17] T.A. Tyson, Q. Qian, C.-C. Kao, J.-P. Rueff, F.M.F. de Groot, M. Croft, S.-W. Cheong, M. Greenblatt, M.A. Subramanian, *Phys. Rev. B* 60 (1999) 4665.
- [18] (a) D.C. Konningsberger, R. Prins (Eds.), *X-Ray Absorption: Principles, Applications, Techniques of EXAFS, SEXAFS and XANES*, Wiley, New York, 1988;  
(b) P.A. Lee, P.H. Citrin, P. Eisenberger, B.M. Kincaid, *Rev. Mod. Phys.* 53 (1981) 679.
- [19] (a) Q. Qian, T.A. Tyson, C.-C. Kao, M. Croft, A.Y. Ignatov, *Appl. Phys. Lett.* 80 (2002) 3141;  
(b) Q. Qian, T.A. Tyson, S. Savrassov, C.C. Kao, M. Croft, *Phys. Rev. B* 68 (2003) 014429.
- [20] R. Kajimoto, Ph. D. Thesis, unpublished.
- [21] Q. Qian, T.A. Tyson, C.-C. Kao, W. Prellier, J. Bai, A. Biswas, R.L. Greene, *Phys. Rev. B* 63 (2001) 224424.
- [22] M.v. Zimmermann, J.P. Hill, D. Gibbs, M. Blume, D. Casa, B. Keimer, Y. Murakami, Y. Tomioka, Y. Tokura, *Phys. Rev. Lett.* 83 (1999) 4872;  
Y. Murakami, J.P. Hill, D. Gibbs, M. Blume, I. Koyama, M. Tanaka, H. Kawata, T. Arima, Y. Tokura, K. Hirota, Y. Endoh, *Phys. Rev. Lett.* 81 (1998) 582.